

Received January 15, 2020, accepted February 24, 2020, date of publication March 2, 2020, date of current version March 11, 2020.

Digital Object Identifier 10.1109/ACCESS.2020.2977429

Prediction of the Remaining Useful Life of Lithium-Ion Batteries Based on Empirical Mode Decomposition and Deep Neural Networks

JIANSHU QIAO¹, XIAOFENG LIU¹, AND ZEHUA CHEN¹

College of Data Science, Taiyuan University of Technology, Taiyuan 030600, China

Corresponding author: Zehua Chen (zehuachen@163.com)

This work was supported by the Key Research and Development Projects of Shanxi Province under Grant 201603D112002.

ABSTRACT The prediction of the remaining useful life (RUL) of lithium-ion batteries (LIBs) is vital for the battery management system used in electric vehicles. We can avoid unnecessary losses if we can accurately predict the RUL of batteries and replace batteries on time. This study proposes a method for predicting the RUL of LIBs based on empirical mode decomposition, deep neural network (DNN), and the long short-term memory model. We then extract the discharge data of LIBs. Subsequently, by applying empirical mode decomposition, the dischargeable capacity of the LIBs is decomposed into a global deterioration trend and capacity regeneration. The long short-term memory model is then applied to predict capacity regeneration, while DNNs predict global deterioration trend. Finally, we add the individual predicted results to obtain the dischargeable capacity of the LIBs; consequently, we obtain the RUL of the LIBs. The proposed method yields a more accurate prediction result than the mixed model of empirical mode decomposition and autoregressive integrated moving average model.

INDEX TERMS Deep neural network, empirical mode decomposition, lithium-ion batteries, remaining useful life.

I. INTRODUCTION

Lithium-ion batteries (LIBs) have the advantages of high energy density, no memory effect, and long lifetimes compared with lead-acid or nickel-metal hydride batteries; therefore, they are extensively used in mobile phones, computers, and electric vehicles [1], [2]. However, owing to a series of physical and chemical changes occurring inside the LIB, its discharge capacity gradually reduces during the long-term charge and discharge processes, i.e., its state of health (SOH) gradually decreases [3]. Casualties may occur when a LIB's SOH drops to a certain level [4], [5]. Therefore, it is vital to accurately predict the remaining useful life (RUL) of the LIB. The definition of LIB's SOH is the ratio of the present cycle's maximum dischargeable capacity to the rated capacity of the battery [6]. The LIB's RUL refers to the number of cycles of the remaining battery before the SOH reaches the threshold [7]. Presently, typical research methods include model-based and data-driven approaches [8].

The associate editor coordinating the review of this manuscript and approving it for publication was Jenny Mahoney.

Model-based approaches capture the long-term dependence of battery capacity deterioration with mathematical formulas to predict the battery's RUL [9]. The most extensively applied of these formulas is the particle filtering (PF) algorithm and its improved algorithms [10]–[14]. Guha and Patra [10] first designed an empirical model using battery data and applied the empirical model to the PF framework to predict the battery's RUL. Dong *et al.* [11] investigated the influence of the motion distance of Brownian particles on a battery's capacity deterioration at a specific time interval. They used a particle filter to estimate the motion parameters of Brownian motion to the battery's RUL. Mo *et al.* [12] introduced a combination of the Kalman filter and standard PF to improve the estimation accuracy; moreover, to predict the RUL, they combined the particle swarm optimization algorithm to slow the particle degradation caused by particle resampling. Zhang *et al.* [13] utilized the Markov chain Monte Carlo algorithm to solve the problem of sample starvation in the improved unscented particle filter (IUPF) algorithm. Furthermore, the IUPF method is proposed based on the unscented particle filter; therefore, it can suppress the particle's existing degradation in the standard PF algorithm,

thus improving the prediction accuracy. Wang *et al.* [14] established a state-space model of LIB capacity for determining capacity degradation. The state-space model can be extrapolated to the specified fault threshold once the state-space model is determined. Then, they get the LIB's RUL. Even though the model-based approach has recently made significant progress, it still has several limitations: i) model-based algorithms are not universal [15] and ii) the use of filtering techniques to predict the accuracy of RUL depends on the parameters of the model [16].

The data-driven approach does not care about the internal reaction of the battery and its parameters; it extracts essential information from the battery's historical data to evaluate the battery's capacity decay law [17]. Du *et al.* [18] used a support vector regression model to model the temperature and charge and discharge power and battery capacity; subsequently, they utilized the established model to predict the battery's RUL. Song *et al.* [19] combined a convolutional neural network (CNN) and the long short-term memory model to infer the battery state of charge (SOC) from the measured data to predict SOH. Li *et al.* [20] proposed deep belief networks to train the historical capacity data of the battery; they predicted the battery's SOH to obtain the battery's RUL. Li *et al.* [21] initially used empirical mode decomposition (EMD) to decompose the recorded battery capacity into several sub-layers and subsequently used recurrent long short-term memory model and Elman NNs to predict sub-layers and finally obtained the RUL. Zhang *et al.* [22] utilized long short-term memory models to discuss the long-term dependance of the capacity of LIBs; subsequently, they combined the Monte Carlo simulation to predict the RUL of multiple LIBs at various temperatures.

LIBs suffer from sudden, momentary, and occasionally considerable capacity regeneration. This phenomenon is known as self-charging in the logger in which a sudden increment in the available capacity happens at the next cycle [23]. Capacity regeneration, which is related to physicochemical aspects, temperature, and load conditions during charge and discharge cycles is particularly important because it often alters the trend of the SOH curve, thus affecting the performance of SOH estimation and prognosis. Therefore, we need to consider the SOH time series as a mixture of multiple signals [24], [25]. Hence, in this study, we first use EMD to decompose the battery capacity into a global deterioration trend, capacity regeneration. Then, we use the long short-time memory (LSTM) to predict capacity regeneration because it can capture the nonlinear relationship between data compared with the autoregressive integrated moving average model (ARIMA) [25]. Moreover, we introduce the current-voltage, temperature, and time characteristics of the battery with the deep NN (DNN) to predict the global deterioration trend of the battery's capacity. Furthermore, the prediction results demonstrate the better performance of our proposed prediction method compared with other methods.

II. RELATED ALGORITHMS

A. EMD

The EMD method proposed by Zhang *et al.* [26] is a new type of adaptive signal time-frequency processing method; it performs signal decomposition based on the time-scale characteristics of the data and decomposes complex signals into a finite intrinsic-mode function (IMF). Moreover, it does not require any basic functions in advance, and this is fundamentally different from the Fourier and wavelet decompositions [28].

In EMD, the data $x(t)$ are decomposed into the IMFs and residue terms, as presented in (1).

$$x(t) = \sum_{j=1}^n c_j(t) + r_n(t) \quad (1)$$

where $c_j(t)$ ($j = 1, 2, \dots, n$) is the IMF in different decompositions, $r_n(t)$ is the residue, and n is the number of IMFs.

The EMD procedure can be given as follows:

Step 1: Identify all the local extreme values of the time series $x(t)$, including the local maxima and minima.

Step 2: Connect all the local maxima and minima with a cubic spline as the upper and lower envelope, respectively. Denote the upper envelope as $x_u(t)$ and the lower envelope as $x_l(t)$.

Step 3: Compute the mean envelope from the upper and lower envelopes, as presented in (2).

$$m(t) = [x_l(t) + x_u(t)]/2 \quad (2)$$

Step 4: Extract the IMF, as presented in (3).

$$h(t) = x(t) - m(t) \quad (3)$$

Step 5: Judge whether the termination criterion is satisfied. If yes, output $x(t)$ as the residue $r_n(t)$, and stop the EMD calculation. Otherwise, go to step 6.

Step 6: Accept $h(t)$ as one of the IMFs, as presented in (4).

$$c_j(t) = h(t) \quad (4)$$

Step 7: Replace $x(t)$ with the residue $r(t)$, as presented in (5); subsequently, then go to step 1.

$$r(t) = x(t) - c_j(t) \quad (5)$$

Note that the termination criterion used in step 5 is set as in (6).

$$\sum_{t=1}^N \frac{[h_{j-1}(t) - h_j(t)]^2}{h_{j-1}^2(t)} \leq \delta, \quad j=1, 2, \dots, N \quad t=1, 2, \dots, N. \quad (6)$$

where N is the number of SOH data points, δ is the termination parameter, and j is the number of iterative calculations. In this study, δ is equal to 0.05.

B. DNN

DNN is a supervised network, so it needs the input and output data of the model during the training phase [32]. It does not specify the number of hidden layers and that of neurons, and you can choose the appropriate one based on your needs. There is no limit to the number of neurons in the output layer. Moreover, the DNN needs to initialize the weight between the networks, and then the process of learning is to continually adjust the weights to obtain the desired output [29]. Fig. 1 shows the brief model of the DNN.

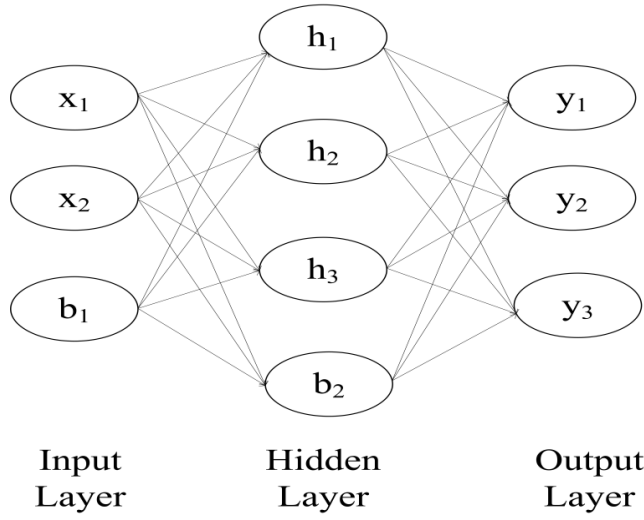


FIGURE 1. DNN model.

where $\{x_1, x_2\}$ denotes input data; b_1 denotes the deviation from the input layer to the hidden layer; $\{h_1, h_2, h_3\}$ denotes neuron node; b_2 denotes hidden layer; $\{y_1, y_2, y_3\}$ denotes the output of the neuron.

The calculation formula from the input layer to the hidden layer is given in (7).

$$h_j = f(x_i w_{ij} + b_j) \quad i = 1, 2, \dots, n; j = 1, 2, \dots, n. \quad (7)$$

where f denotes activation function, x_i denotes input of the input layer, and w_{ij} denotes the weight of the input layer to the hidden layer, indicating the deviation of the input layer to the hidden layer. “ i ” denotes the number of neurons in the input layer, “ j ” denotes the number of neurons in the hidden layer, and h_j denotes the neuron node of the hidden layer.

The calculation formula from the hidden layer to the output layer is as shown in (8).

$$y_k = f(h_j w_{jk} + b_k) \quad k = 1, 2, \dots, n; j = 1, 2, \dots, n. \quad (8)$$

where f denotes the activation function, h_j denotes the input of the output layer, w_{jk} denotes the weight of the hidden layer to the output layer, and b_k denotes the deviation of the input layer to the hidden layer. “ j ” denotes the number of neurons in the hidden layer, “ k ” denotes the number of neurons in the output layer, and y_k denotes the output of the NN.

The calculated output of the NN is compared with the label in the dataset to calculate the loss function. Then,

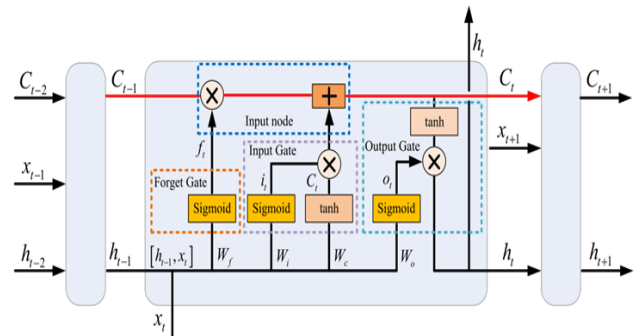


FIGURE 2. LSTM model.

the optimization algorithm is applied to minimize the loss function and finally obtain the optimal weight and deviation.

C. LSTM

Fig. 2 [30] shows the basic structure of the LSTM model, where h_{t-1} denotes the output of the previous moment, c_{t-1} denotes the memory unit of the previous time, h_t denotes the output of the current time step, and c_t denotes the memory unit of the current time. The red line, which is the core of LSTM, is utilized to convey information and does not change throughout the process. The LSTM model comprises the forget, input, and output gates.

The forget gates choose to forget some past information, as in (9):

$$f_t = \sigma(W_f \cdot [h_{t-1}, x_t] + b_f) \quad (9)$$

The input gate is applied to select some of the present memory information, as presented in (10) and (11):

$$i_t = \sigma(W_i \cdot [h_{t-1}, x_t] + b_i) \quad (10)$$

$$\tilde{C}_t = \tanh(W_c \cdot [h_{t-1}, x_t] + b_c) \quad (11)$$

Equation (12) combines past information with current information.

$$C_t = f_t * C_{t-1} + i_t * \tilde{C}_t \quad (12)$$

The output gate is utilized to output the result, as presented in (13) and (14).

$$o_t = \sigma(W_o \cdot [h_{t-1}, x_t] + b_o) \quad (13)$$

$$h_t = o_t * \tanh(C_t) \quad (14)$$

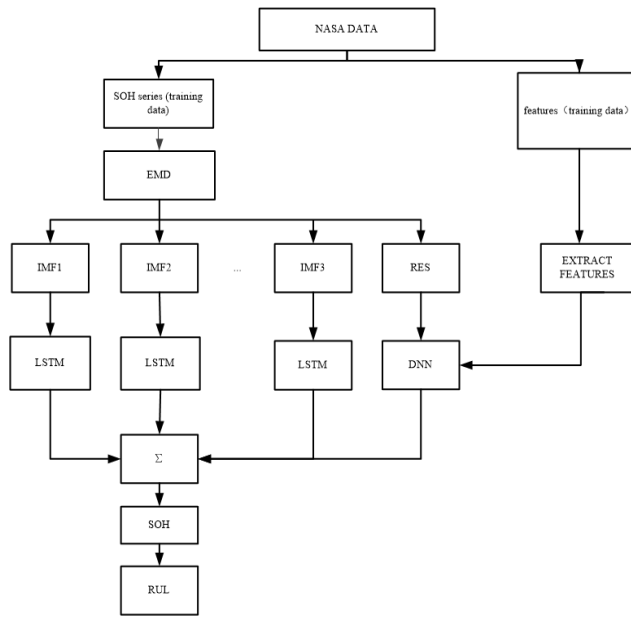
D. PROPOSED METHOD

Fig. 3 shows the details of a battery’s SOH prediction steps.

Step 1: We obtain the original dischargeable capacity sequence, current, and voltage temperatures of the LIB and their corresponding times.

Step 2: We select the number of training sets and use EMD to decompose the SOH of the training set into capacity regenerative IMFs and global descent trend RES.

Step 3: We train the LSTM model with part data of IMFs and train the DNN model with part data of features and RES. Finally, we use the trained model to predict the following data separately.

**FIGURE 3.** RUL prediction procedure.

Step 4: We add all the separate prediction results to obtain the SOH and subsequently calculate the RUL.

III. PROGNOSTIC EXPERIMENT

A. EXPERIMENTAL DATA

The experimental data used in this study were obtained from data repository of the NASA Ames Prognostics Center of Excellence (PCoE) [31]. Life-cycle tests were conducted on 18,650-size LIBs at a battery testbed. The testbed contains a power supply, programmable direct current electronic, voltmeter, thermocouple sensor, environmental chamber, and an electrochemical impedance spectroscopy. The cathode and anode materials of the LIBs are mostly MAG-10 graphite And Li_{0.8}iCo_{0.15}Al_{0.05}O₂, respectively, and the failure threshold was 70%. The testbed comprises four different batteries (5, 6, 7, 18) and the following three different operations for each LIB at room temperature (24): charging, discharging, and resistance testing as described below.

Charging Step: The charging was first performed at a constant current (CC) 1.5 A until the charging voltage reached 4.2 V. Then, the charging was changed to the constant voltage mode until the charging current dropped to 20 mA.

Discharging Step: This was performed using the CC mode until a predefined cutoff voltage was reached.

Impedance Measurement: Measurement was performed using an electrochemical impedance spectroscopy frequency ranging from 0.1 to 5 kHz with repeated charging and discharging to accelerate battery aging, which ended when the battery discharging capacity dropped to 70% of its rated capacity (2 Ah).

Consequently, charging and discharging are repeatedly performed to accelerate battery aging, and the experiment ends when the battery discharging capacity drops to 70% of rated capacity (2 Ah).

TABLE 1. Attributes for discharging step.

Attributes	Explanation
Voltage_measured	Battery terminal voltage
Current_measured	Battery output current
Temperature_measured	Battery temperature
Current_charge	Current measured at load
Voltage_charge	Voltage measured at load
Time	Time vector for the cycle
Capacity	Battery capacity

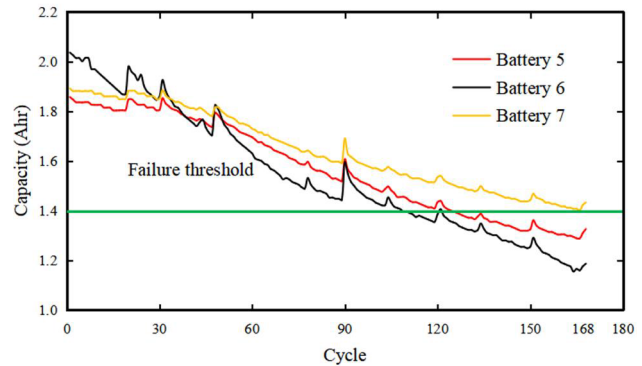
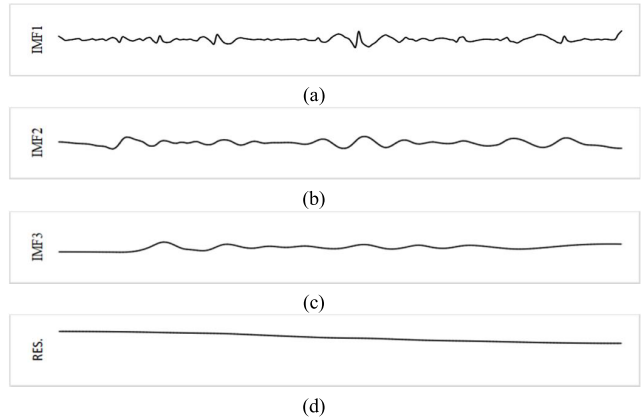
**FIGURE 4.** Capacity of battery No. 5–7.**FIGURE 5.** SOH decomposition of battery 5 by EMD. (a) IMF1. (b) IMF2. (c) IMF3. (d) RES.

Table 1 shows the discharging attributes of data repository of the NASA.

Fig. 4 shows the variation of the discharging capacity of the battery as the number of cycles increases. Fig. 5 shows the decomposition results of the EMD using a No. 5 battery as an example. IMF1 and IMF2 had high fluctuations, while IMF3 had relatively low fluctuations corresponding to the capacity regeneration. RES can genuinely describe the downward trend of the battery; therefore, we can use RES to describe the discharging capacity of the battery.

B. EXTRACT FEATURES

This study primarily extracted the current, voltage, temperature, and time data in each cycle of batteries during the discharging process as a feature based on a single cycle. The extraction method is as in (14)-(16) [32].

$$(t, v) = \{(t_i, v_i) | \min(v_i)\} \quad i = 1, 2, 3, \dots, n. \quad (15)$$

where v denotes the minimum value of the voltage, t denotes the time corresponding to the minimum value of the voltage,

$$(t_{\min\{i\}}, A) \text{ s.t } A_i > -2A \quad i = 1, 2, 3, \dots, n. \quad (16)$$

And A denotes the time corresponding to the current value before the current starts to rise by $2A$. $t_{\min\{i\}}$ denotes the time,

$$(t, T) = \{(t_i, T_i) | \max(T_i)\} \quad i = 1, 2, 3, \dots, n. \quad (17)$$

where T denotes the maximum value of temperature, and t denotes its corresponding time.

C. PROGNOSTIC RESULT AND ANALYSIS

1) EVALUATION CRITERIA

Before the RUL prediction, the definition of the absolute error (AE) and root mean squared error (RMSE) as the evaluation criteria for the prediction performance as follows:

a) AE can be defined as follows:

$$AE = |T - P| \quad (18)$$

b) RMSE can be defined as follows:

$$RMSE = \sqrt{\frac{1}{n} \sum_{i=1}^n [T_{i+s} - P_{i+s}]^2} \quad (19)$$

where n denotes the number of predict results, P denotes the value of the predicted SOH; s denotes the starting cycle; T_{i+s} denotes the actual SOH; and P_{i+s} denotes the predicted SOH.

2) PROGNOSTIC DESIGN

For the LSTM model, we set two batches for training. The size of each batch is 32, the hidden layer size is 200, and the number of the training times is 400. Based on the evaluation data and backward prediction, the model was evaluated; the number of prediction data varied with the prediction starting point. The DNN sets up two layers of a hidden-layer network; the nodes of the hidden layer were 32 and 8, and the number of neurons in the output layer was 1. The loss function used the mean square error, optimizer used ADAM, and training times were adjusted based on the conducted experiments. Then, we conducted the experiments on battery No. 5, 6, and 7.

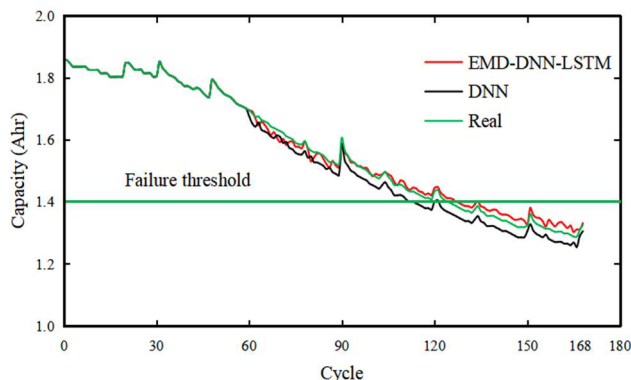


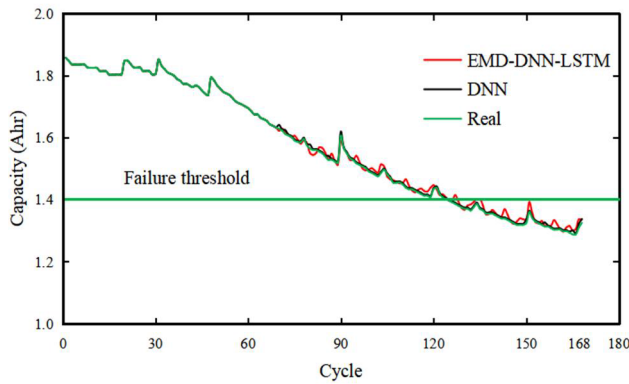
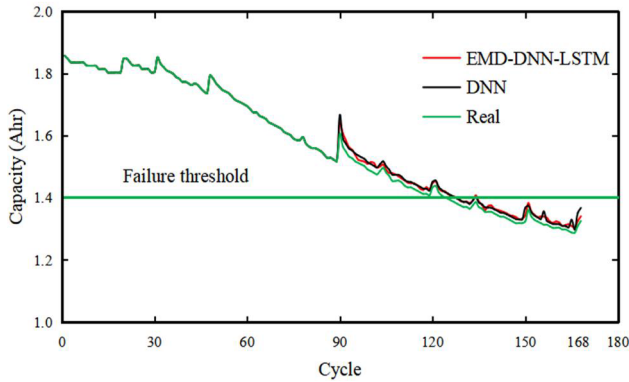
FIGURE 6. RUL prediction for battery No. 5 after 60 cycles.

TABLE 2. RUL prediction performance with EMD-DNN-LSTM compared with that in case of other methods.

Method	No.	Start point	Real RUL	Predicted RUL	AE	RMSE
EMD-DNN-LSTM	5	60	65	67	2	0.0008
		70	55	55	0	0.0008
		80	45	29	0	0.0007
		90	35	39	4	0.0016
		100	25	25	0	0.0009
	6	50	59	61	2	0.0014
		60	49	52	3	0.0040
		70	39	36	3	0.0024
		80	29	29	0	0.0037
		90	19	20	1	0.0034
EMD-ARMA	7	90	78	78	0	0.0021
		100	68	68	0	0.0004
		110	58	58	0	0.0006
		120	48	48	0	0.0014
		130	38	38	0	0.0021
	5	60	65	73	8	0.0209
		70	55	70	15	0.0171
		80	45	46	1	0.0108
		90	35	48	13	0.0195
		100	25	29	4	0.0075
DNN	6	50	59	61	2	0.0389
		60	49	50	1	0.0504
		70	39	40	1	0.0224
		80	29	32	3	0.0171
		90	19	19	0	0.0285
	7	90	76	68	2	0.0113
		100	66	64	2	0.0094
		110	56	52	4	0.0079
		120	46	38	8	0.0080
		130	36	34	2	0.0098
ARIMA	5	60	65	61	4	0.0314
		70	55	55	0	0.005
		80	45	46	1	0.0109
		90	35	37	2	0.0208
		100	25	21	4	0.0045
	6	50	59	61	2	0.0281
		60	49	44	5	0.0220
		70	39	34	5	0.0195
		80	29	30	1	0.0079
		90	19	20	1	0.0042
R-RVM	7	90	78	78	0	0.0317
		100	68	68	0	0.0026
		110	58	58	0	0.0096
		120	48	48	0	0.0027
		130	38	33	5	0.0099
	5	60	65	53	12	0.0127
		70	55	35	20	0.0235
		80	45	29	16	0.0214
		90	35	64	29	0.0376
		100	25	18	7	0.0061
6	6	50	59	75	16	0.0491
		60	49	34	15	0.0244
		70	39	18	21	0.0168
		80	29	13	16	0.0382
		90	19	34	15	0.0267
	7	90	76	243	167	/
		100	66	51	15	0.0113
		110	56	46	10	0.0090
		120	46	66	20	/
		130	36	25	11	0.0113
5	6	60	65	74	9	/
		80	45	52	7	/
	6	60	49	50	1	/
		80	29	35	6	/

3) RESULT ANALYSIS

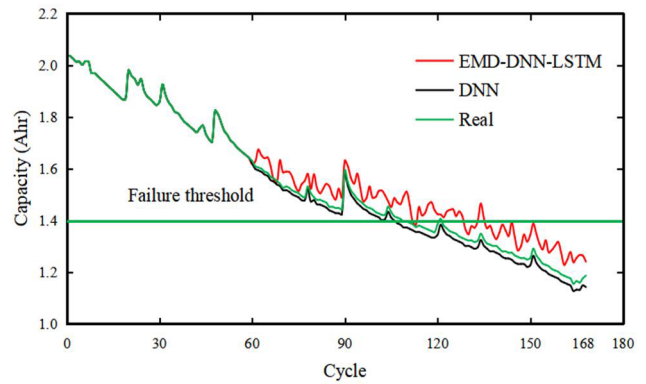
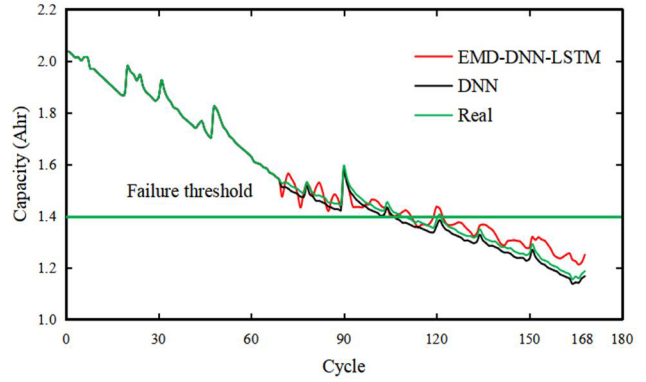
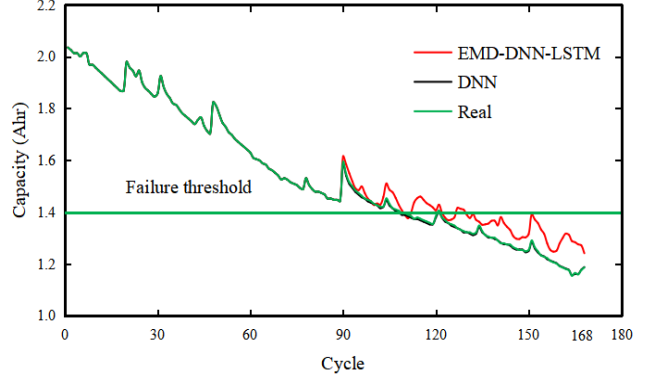
Table 2 presents the comparison results between the algorithm and other methods [33]. We conducted the experiments on battery No. 5, 6, and 7 at five different starting points. Fig. 6–12 show the experimental results.

**FIGURE 7.** RUL prediction for battery No. 5 after 70 cycles.**FIGURE 8.** RUL prediction for battery No. 5 after 90 cycles.**TABLE 3.** RUL prediction performance with EMD-DNN-LSTM compared with that in case of other methods at same cycles.

Cycle	Method	Battery No. 5		Battery No. 6	
		AE	RMSE	AE	RMSE
60	EMD-DNN-LSTM	2	0.0008	3	0.0040
	EMD-ARMA	8	0.0209	1	0.0504
	DNN	4	0.0314	5	0.0220
	ARIMA	12	0.0127	15	0.0244
70	EMD-DNN-LSTM	0	0.0008	3	0.0024
	EMD-ARMA	15	0.0171	1	0.0224
	DNN	1	0.0050	5	0.0195
	ARIMA	20	0.0235	21	0.0168
80	EMD-DNN-LSTM	0	0.0007	0	0.0037
	EMD-ARMA	1	0.0108	3	0.0171
	DNN	1	0.0109	1	0.0079
	ARIMA	16	0.0214	16	0.0382
90	EMD-DNN-LSTM	4	0.0016	1	0.0034
	EMD-ARMA	13	0.0195	0	0.0285
	DNN	2	0.0208	1	0.0042
	ARIMA	29	0.0376	15	0.0267

As demonstrated in Fig. 6–12 and Table 2, the AE of EMD–LSTM–DNN is lesser than that of EMD–ARMA. The maximum, minimum, and average values of the AE of EMD–LSTM–DNN is 4, 0, and 1, respectively, whereas those of the EMD–ARMA are 15, 0, and 4.4, respectively. Therefore, in this study, the algorithm is relatively stable and accurate.

The RMSE of EMD–LSTM–DNN is lesser than that of EMD–ARMA, and the maximum, minimum, and average

**FIGURE 9.** RUL prediction for battery No. 6 after 60 cycles.**FIGURE 10.** RUL prediction for battery No. 6 after 70 cycles.**FIGURE 11.** RUL prediction for battery No. 6 after 90 cycles.

values of AE of EMD–LSTM–DNN are 0.004, 0.0004, 0.0017, respectively. All the values were minimal, indicating that the algorithm can better predict the SOH of the battery. Therefore, we can conclude that the proposed algorithm can effectively predict the SOH of the battery and accurately predict the battery's RUL.

As shown in Fig. 6–12 and Table 3, the average values of the AE of EMD–LSTM–DNN are lesser than that of EMD–ARMA in the same cycles. Moreover, the average values of the AE of EMD–LSTM–DNN are 2.5, 1.5, 0, 2.5, respectively, whereas those of the EMD–ARMA are 4.5, 8, 2.5 and 6.5, respectively. Therefore, in this study, the algorithm is relatively stable and accurate.

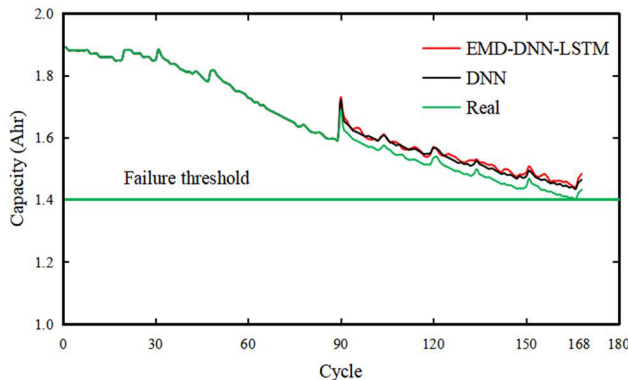


FIGURE 12. RUL prediction for battery No. 7 after 90 cycles.

The RMSE of EMD–LSTM–DNN is lesser than that of EMD–ARMA, and the average values of RMSE of EMD–LSTM–DNN are 0.0024, 0.0016, 0.0022, 0.0025, whereas those of the EMD–ARMA are 0.03565, 0.01975, 0.01395 and 0.024, respectively. All the values were minimal, indicating that the algorithm can better predict the SOH of the battery.

IV. CONCLUSION

The contributions of this study can be summarized as follows.

a) The global deterioration trend and capacity regeneration obtained by decomposing SOH using EMD does not lose the characteristics of the original dischargeable capacity. After decomposition, the method proposed in this study was used for prediction, and the averages of AE and RMSE decreased by 75% and 90.8%, respectively. Therefore, the application of the algorithm proposed in this study can effectively improve the accuracy of prediction.

b) Herein, the proposed algorithm has a prediction of <5 in 15 RULs; only 73% of EMD–ARIMA is >5 . The standard deviation of RUL for EMD–ARIMA was 4.40908 in the 15 conducted experiments, whereas the standard deviation of RUL for the algorithm was 1.36626. Therefore, the RUL value predicted by the algorithm is more stable.

In this study, we extracted the multi-scale information of the original capacity data by applying the EMD algorithm, and the capacity fluctuation and global downward trend are

predicted using different methods. Using DNN, the prediction of RES can predict the correspondence between the characteristics of current and voltage and the RES of the battery under a specific cycle. The LSTM model is applied to predict the IMFS with distinct timing characteristics. Moreover, we reasonably predicted the battery's RUL from the horizontal and vertical directions for different decomposition contents, and the proposed method can accurately and effectively predict the battery's SOH and RUL. However, we cannot obtain more battery data because the operation is tedious and complicated. The condition of the conducted experiment is limited. Furthermore, EMD has

the end effect problem, the stopping condition of IMFS screening, and modal aliasing, which influence the experimental results. Therefore, in a future work, we will discuss

battery data based on various conditions and experiments on different types of batteries. Generative adversarial network (GAN) can generate new data with the same statistics as the training set, which can improve the accuracy of predicting model. Furthermore, it is better to find a solution to solve the problems of EMD. Moreover, algorithm fusion is a good trend; therefore, it is not a bad idea to introduce some mature, stable, and robust prognostic methods to the LIBs' RUL prediction.

REFERENCES

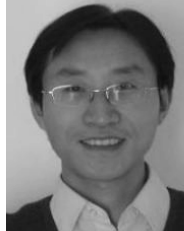
- [1] D. Wang, F. Yang, Y. Zhao, and K.-L. Tsui, "Battery remaining useful life prediction at different discharge rates," *Microelectron. Rel.*, vol. 78, pp. 212–219, Nov. 2017, doi: [10.1016/j.microrel.2017.09.009](https://doi.org/10.1016/j.microrel.2017.09.009).
- [2] P. Khumprom and N. Yodo, "A data-driven predictive prognostic model for lithium-ion batteries based on a deep learning algorithm," *Energies*, vol. 12, no. 4, p. 660, Feb. 2019, doi: [10.3390/en12040660](https://doi.org/10.3390/en12040660).
- [3] Y. Zhang, R. Xiong, H. He, and M. Pecht, "Validation and verification of a hybrid method for remaining useful life prediction of lithium-ion batteries," *J. Cleaner Prod.*, vol. 212, pp. 240–249, Mar. 2019, doi: [10.1016/j.jclepro.2018.12.041](https://doi.org/10.1016/j.jclepro.2018.12.041).
- [4] X. H. Su, S. Wang, M. Pecht, L. L. Zhao, and Z. Ye, "Interacting multiple model particle filter for prognostics of lithium-ion batteries," *Microelectron. Rel.*, vol. 70, pp. 59–69, Mar. 2017, doi: [10.1016/j.microrel.2017.02.003](https://doi.org/10.1016/j.microrel.2017.02.003).
- [5] Q. Zhao, X. Qin, H. Zhao, and W. Feng, "A novel prediction method based on the support vector regression for the remaining useful life of lithium-ion batteries," *Microelectron. Rel.*, vol. 85, pp. 99–108, Jun. 2018, doi: [10.1016/j.microrel.2018.04.007](https://doi.org/10.1016/j.microrel.2018.04.007).
- [6] D. Wang, F. Yang, Y. Zhao, and K.-L. Tsui, "Prognostics of lithium-ion batteries based on state space modeling with heterogeneous noise variances," *Microelectron. Rel.*, vol. 75, pp. 1–8, Aug. 2017, doi: [10.1016/j.microrel.2017.06.002](https://doi.org/10.1016/j.microrel.2017.06.002).
- [7] F. Yang, D. Wang, Y. Xing, and K.-L. Tsui, "Prognostics of Li(NiMnCo)O₂-based lithium-ion batteries using a novel battery degradation model," *Microelectron. Rel.*, vol. 70, pp. 70–78, Mar. 2017, doi: [10.1016/j.microrel.2017.02.002](https://doi.org/10.1016/j.microrel.2017.02.002).
- [8] K. Pugalenth and N. Raghavan, "A holistic comparison of the different resampling algorithms for particle filter based prognosis using lithium ion batteries as a case study," *Microelectron. Rel.*, vol. 91, pp. 160–169, Dec. 2018, doi: [10.1016/j.microrel.2018.08.007](https://doi.org/10.1016/j.microrel.2018.08.007).
- [9] Y. Peng, Y. Hou, Y. Song, J. Pang, and D. Liu, "Lithium-ion battery prognostics with hybrid Gaussian process function regression," *Energies*, vol. 11, no. 6, p. 1420, Jun. 2018, doi: [10.3390/en11061420](https://doi.org/10.3390/en11061420).
- [10] A. Guha and A. Patra, "Particle filtering based estimation of remaining useful life of lithium-ion batteries employing power fading data," in *Proc. IEEE Int. Conf. Prognostics Health Manage.*, Dallas, TX, USA, Jun. 2017, pp. 193–198, doi: [10.1109/ICPHM.2016.7542847](https://doi.org/10.1109/ICPHM.2016.7542847).
- [11] G. Dong, Z. Chen, J. Wei, and Q. Ling, "Battery health prognosis using brownian motion modeling and particle filtering," *IEEE Trans. Ind. Electron.*, vol. 65, no. 11, pp. 8646–8655, Nov. 2018, doi: [10.1109/TIE.2018.2813964](https://doi.org/10.1109/TIE.2018.2813964).
- [12] B. Mo, J. Yu, D. Tang, H. Liu, and J. Yu, "A remaining useful life prediction approach for lithium-ion batteries using Kalman filter and an improved particle filter," in *Proc. IEEE Int. Conf. Prognostics Health Manage. (ICPHM)*, Ottawa, ON, Canada, Jun. 2016, pp. 1–5, doi: [10.1109/ICPHM.2016.7542847](https://doi.org/10.1109/ICPHM.2016.7542847).
- [13] X. Zhang, Q. Miao, and Z. Liu, "Remaining useful life prediction of lithium-ion battery using an improved UPF method based on MCMC," *Microelectron. Rel.*, vol. 75, pp. 288–295, Aug. 2017, doi: [10.1016/j.microrel.2017.02.012](https://doi.org/10.1016/j.microrel.2017.02.012).
- [14] D. Wang, F. Yang, K.-L. Tsui, Q. Zhou, and S. J. Bae, "Remaining useful life prediction of lithium-ion batteries based on spherical cubature particle filter," *IEEE Trans. Instrum. Meas.*, vol. 65, no. 6, pp. 1282–1291, Jun. 2016, doi: [10.1109/TIM.2016.2534258](https://doi.org/10.1109/TIM.2016.2534258).
- [15] R. Xiong, Y. Zhang, H. He, X. Zhou, and M. G. Pecht, "A double-scale, particle-filtering, energy state prediction algorithm for lithium-ion batteries," *IEEE Trans. Ind. Electron.*, vol. 65, no. 2, pp. 1526–1538, Feb. 2018, doi: [10.1109/TIE.2017.2733475](https://doi.org/10.1109/TIE.2017.2733475).

- [16] P. L. T. Duong and N. Raghavan, "Heuristic Kalman optimized particle filter for remaining useful life prediction of lithium-ion battery," *Microelectron. Rel.*, vol. 81, pp. 232–243, Feb. 2018, doi: [10.1016/j.microrel.2017.12.028](https://doi.org/10.1016/j.microrel.2017.12.028).
- [17] Y. Song, D. Liu, C. Yang, and Y. Peng, "Data-driven hybrid remaining useful life estimation approach for spacecraft lithium-ion battery," *Microelectron. Rel.*, vol. 75, pp. 142–153, Aug. 2017, doi: [10.1016/j.microrel.2017.06.045](https://doi.org/10.1016/j.microrel.2017.06.045).
- [18] J. Du, W. Zhang, C. Zhang, and X. Zhou, "Battery remaining useful life prediction under coupling stress based on support vector regression," *Energy Procedia*, vol. 152, pp. 538–543, Oct. 2018, doi: [10.1016/j.egypro.2018.09.207](https://doi.org/10.1016/j.egypro.2018.09.207).
- [19] X. Song, F. Yang, D. Wang, and K.-L. Tsui, "Combined CNN-LSTM network for State-of-Charge estimation of lithium-ion batteries," *IEEE Access*, vol. 7, pp. 88894–88902, Jul. 2019, doi: [10.1109/ACCESS.2019.2926517](https://doi.org/10.1109/ACCESS.2019.2926517).
- [20] L. Li, Y. Peng, Y. Song, and D. Liu, "Lithium-ion battery remaining useful life prognostics using data-driven deep learning algorithm," in *Proc. Prognostics Syst. Health Manage. Conf. (PHM-Chongqing)*, Chongqing, China, Oct. 2018, pp. 1094–1100, doi: [10.1109/PHM-Chongqing.2018.00193](https://doi.org/10.1109/PHM-Chongqing.2018.00193).
- [21] X. Li, L. Zhang, Z. Wang, and P. Dong, "Remaining useful life prediction for lithium-ion batteries based on a hybrid model combining the long short-term memory and elman neural networks," *J. Energy Storage*, vol. 21, pp. 510–518, Feb. 2019, doi: [10.1016/j.est.2018.12.011](https://doi.org/10.1016/j.est.2018.12.011).
- [22] Y. Zhang, R. Xiong, H. He, and M. G. Pecht, "Long short-term memory recurrent neural network for remaining useful life prediction of lithium-ion batteries," *IEEE Trans. Veh. Technol.*, vol. 67, no. 7, pp. 5695–5705, Jul. 2018, doi: [10.1109/TVT.2018.2805189](https://doi.org/10.1109/TVT.2018.2805189).
- [23] Y. Q. Sun, X. L. Hao, M. Pecht, and Y. P. Zhou, "Remaining useful life prediction for lithium-ion batteries based on an integrated health indicator," *Microelectron. Rel.*, vol. 88, pp. 1189–1194, Sep. 2018, doi: [10.1016/j.microrel.2018.07.047](https://doi.org/10.1016/j.microrel.2018.07.047).
- [24] H. Zhang, Q. Miao, X. Zhang, and Z. W. Liu, "An improved unscented particle filter approach for lithium-ion battery remaining useful life prediction," *Microelectron. Rel.*, vol. 88, pp. 288–298, Feb. 2018, doi: [10.1016/j.microrel.2017.12.036](https://doi.org/10.1016/j.microrel.2017.12.036).
- [25] Y. Chang, H. Fang, and Y. Zhang, "A new hybrid method for the prediction of the remaining useful life of a lithium-ion battery," *Appl. Energy*, vol. 206, pp. 1564–1578, Nov. 2017, doi: [10.1016/j.apenergy.2017.09.106](https://doi.org/10.1016/j.apenergy.2017.09.106).
- [26] Y. Zhang, R. Xiong, H. He, and Z. Liu, "A LSTM-RNN method for the lithium-ion battery remaining useful life prediction," in *Proc. Prognostics Syst. Health Manage. Conf. (PHM-Harbin)*, Harbin, China, Jul. 2017, pp. 1–4, doi: [10.1109/PHM.2017.8079316](https://doi.org/10.1109/PHM.2017.8079316).
- [27] N. E. Huang, Z. Shen, S. R. Long, M. C. Wu, H. H. Shih, Q. Zheng, N.-C. Yen, C. C. Tung, and H. H. Liu, "The empirical mode decomposition and the Hilbert spectrum for nonlinear and non-stationary time series analysis," *Proc. Roy. Soc. London. A, Math., Phys. Eng. Sci.*, vol. 454, no. 1971, pp. 903–995, Mar. 1998, doi: [10.1098/rspa.1998.0193](https://doi.org/10.1098/rspa.1998.0193).
- [28] C. Zhang, Y. He, L. Yuan, and S. Xiang, "Capacity prognostics of lithium-ion batteries using EMD denoising and multiple kernel RVM," *IEEE Access*, vol. 5, pp. 12061–12070, Jun. 2017, doi: [10.1109/ACCESS.2017.2716353](https://doi.org/10.1109/ACCESS.2017.2716353).
- [29] C. Liu, X. Wang, J. Tan, L. Wang, W. Sun, and W. He, "Discharge voltage time series classification of lithium-ion cells based on deep neural networks," in *Proc. IEEE 4th Int. Conf. Comput. Commun. (ICCC)*, Chengdu, China, Dec. 2018, pp. 2128–2132, doi: [10.1109/Com-Comm.2018.8780824](https://doi.org/10.1109/Com-Comm.2018.8780824).
- [30] C. Wang, N. Lu, S. Wang, Y. Cheng, and B. Jiang, "Dynamic long short-term memory Neural-Network-based indirect Remaining-Useful-Life prognosis for satellite lithium-ion battery," *Appl. Sci.*, vol. 8, no. 11, p. 2078, Oct. 2018, doi: [10.3390/app8112078](https://doi.org/10.3390/app8112078).
- [31] B. Saha and K. Goebel, (2007). *Battery Data Set Distributed by NASA Ames Prognostics Data Repository*. [Online]. Available: <http://ti.arc.nasa.gov/project/prognostic-Dataproxy>
- [32] L. Ren, L. Zhao, S. Hong, S. Zhao, H. Wang, and L. Zhang, "Remaining useful life prediction for lithium-ion battery: A deep learning approach," *IEEE Access*, vol. 6, pp. 50587–50598, 2018, doi: [10.1109/ACCESS.2018.2858856](https://doi.org/10.1109/ACCESS.2018.2858856).
- [33] Y. P. Zhou and M. H. Huang, "Lithium-ion batteries remaining useful life prediction based on a mixture of empirical mode decomposition and ARIMA model," *Microelectron. Rel.*, vol. 65, pp. 265–274, Oct. 2016, doi: [10.1016/j.microrel.2016.07.151](https://doi.org/10.1016/j.microrel.2016.07.151).

JIANSHU QIAO is currently pursuing the master's degree with the College of Data Science, Taiyuan University of Technology, China. His research interests include deep learning and remaining useful life prediction of LIBs.



XIAOFENG LIU received the Ph.D. degree from the Taiyuan University of Technology, China, in 2014. He is currently a Lecturer with the College of Data Science, Taiyuan University of Technology. His research interests include data analysis and machine learning.



ZEHUA CHEN received the Ph.D. degree from the Taiyuan University of Technology, China, in 2007. She is currently a Professor with the College of Data Science, Taiyuan University of Technology. Her research interests include granular computing, data mining, intelligent information process, and industrial big data.

